Syndecan 4 interacts genetically with Vangl2 to regulate neural tube closure and planar cell polarity

Noelia Escobedo[1], Osvaldo Contreras[1], Rosana Muñoz[1], Marjorie Farías[1], Héctor Carrasco[1], Charlotte Hill[1], Uyen Tran[2], Sophie E. Pryor[3], Oliver Wessely[2], Andrew J. Copp[3] and Juan Larraín[1],*

SUMMARY

Syndecan 4 (Sdc4) is a cell-surface heparan sulfate proteoglycan (HSPG) that regulates gastrulation, neural tube closure and directed neural crest migration in *Xenopus* development. To determine whether Sdc4 participates in Wnt/PCP signaling during mouse development, we evaluated a possible interaction between a null mutation of *Sdc4* and the *loop-tail* allele of *Vangl2*. Sdc4 is expressed in multiple tissues, but particularly in the non-neural ectoderm, hindgut and otic vesicles. *Sdc4;Vangl2^{Lp}* compound mutant mice have defective spinal neural tube closure, disrupted orientation of the stereocilia bundles in the cochlea and delayed wound healing, demonstrating a strong genetic interaction. In *Xenopus*, co-injection of suboptimal amounts of Sdc4 and Vangl2 morpholinos resulted in a significantly greater proportion of embryos with defective neural tube closure than each individual morpholino alone. To probe the mechanism of this interaction, we overexpressed or knocked down Vangl2 function in HEK293 cells. The Sdc4 and Vangl2 proteins colocalize, and Vangl2, particularly the Vangl2^{Lp} mutant form, diminishes Sdc4 protein levels. Conversely, Vangl2 knockdown enhances Sdc4 protein levels. Overall HSPG steady-state levels were regulated by Vangl2, suggesting a molecular mechanism for the genetic interaction in which *Vangl2$^{Lp/+}$* enhances the *Sdc4*-null phenotype. This could be mediated via heparan sulfate residues, as *Vangl2$^{Lp/+}$* embryos fail to initiate neural tube closure and develop craniorachischisis (usually seen only in *Vangl2$^{Lp/Lp}$*) when cultured in the presence of chlorate, a sulfation inhibitor. These results demonstrate that Sdc4 can participate in the Wnt/PCP pathway, unveiling its importance during neural tube closure in mammalian embryos.

KEY WORDS: Neural tube defects, Proteoglycans, Wnt planar cell polarity

INTRODUCTION

The Wnt/PCP pathway controls a variety of cellular and developmental processes where coordinated movement and orientation of cells within the plane of an epithelium is required. This pathway regulates the process of convergence and extension (CE) during gastrulation and neurulation (Wallingford et al., 2002; Ybot-Gonzalez et al., 2007), stereocilia orientation during ear morphogenesis, hair follicle orientation, renal tubular elongation and oriented cell division (Gray et al., 2011; Wang and Nathans, 2007). More recently, a role for Wnt/PCP signaling in epidermal wound healing has been described (Caddy et al., 2010).

The PCP pathway was originally discovered in *Drosophila*. Its core components include the transmembrane receptor Frizzled (Fz), the cytoplasmic proteins Disheveled (Dsh/Dvl) and Prickle (Pk), the four-pass transmembrane protein strabismus (Stbm/Vangl2), and the cadherin-like protein Flamingo/Celsr1 (Gray et al., 2011; Wang and Nathans, 2007). PCP signaling in vertebrates, but not in flies, also involves the Wnt ligands Wnt5a and Wnt11 (Gray et al., 2011; Wallingford et al., 2002).

Neurulation is responsible for initial shaping of the central nervous system and formation of the neural tube, the precursor of the brain and spinal cord. Defective neurulation, where neural tube closure is incomplete, can result in neural tube defects (NTD), a group of malformations that affects ~0.5-2 per 1000 pregnancies worldwide. A breakthrough in understanding the genetic mechanism of NTDs was the finding that components of the Wnt/PCP pathway are required for neurulation in vertebrate embryos (Copp et al., 2003; Wallingford and Harland, 2002). Mice, frogs and zebrafish that are defective for Van Gogh-like 2 (Vangl2), the vertebrate ortholog of *Drosophila* Stbm develop NTDs (Copp et al., 2003). Moreover, recent work has identified point mutations in several genes of the PCP pathway specifically in human NTDs (Doudney et al., 2005; Iliescu et al., 2011; Kibar et al., 2007; Robinson et al., 2012), suggesting that the requirement for Wnt/PCP signaling in neural tube closure may be universal among vertebrates.

Syndecan4 (Sdc4) is a cell surface heparan sulfate proteoglycan (HSPG) involved in cell adhesion (Couchman, 2010; Morgan et al., 2007). We have demonstrated that Sdc4 regulates gastrulation, neural tube closure and neural crest-directed migration in *Xenopus* embryos (Muñoz et al., 2006; Matthews et al., 2008). Sdc4 interacts biochemically with Fz7 and Dsh, and is necessary and sufficient to translocate Dsh to the membrane in a fibronectin-dependent manner, supporting its role in non-canonical Wnt signaling (Muñoz et al., 2006). *Sdc4*-null mice have delayed wound healing, impaired angiogenesis and defects in muscle satellite cells, but no apparent early developmental defects have been described (Cornelison et al., 2004; Echtermeyer et al., 2001; Ishiguro et al., 2000).

Here, we studied the expression of Sdc4 and its interaction with Vangl2 in different biological processes. We find that Sdc4 is expressed in the non-neural ectoderm adjacent to the neural tube, in the gut and in the otic vesicle. *Sdc4* interacts genetically with *Vangl2$^{Lp/+}$* to affect spinal neural tube closure, morphogenesis of the cochlea stereocilia and wound healing. Biochemical and cellular experiments demonstrate that Vangl2 regulates Sdc4 steady-state

[1]Center for Aging and Regeneration, Millennium Nucleus in Regenerative Biology, Faculty of Biological Sciences, P. Universidad Católica de Chile, Alameda 340 Santiago, Chile. [2]Cleveland Clinic Foundation, Lerner Research Institute, Department of Cell Biology, 9500 Euclid Avenue/NC10, Cleveland, OH 44195, USA. [3]Neural Development Unit, Institute of Child Health, University College London, 30 Guilford Street, London WC1N 1EH, UK.

*Author for correspondence (jlarrain@bio.puc.cl)

levels, and also affects total levels of HSPG, providing a molecular explanation for the genetic interaction between these two genes. Heparan sulfate residues could mediate the effect of this interaction, as Vangl2$^{Lp/+}$ embryos develop craniorachischisis when sulfation of the glycosaminoglycan chains is inhibited.

MATERIALS AND METHODS
Animal procedures
Genotyping of the targeted *Sdc4* alleles was performed by PCR of genomic DNA using the following primers: wild-type allele (forward, 5′-CAGG-GCAGCAACATCTTTGAGAGAAC-3′; reverse, 5′-TCCTTCCCATTT-CACAGAGC-3′); and the null allele (forward, 5′-CGCCTTCTTG-ACGAGTTCTT-3′; reverse, 5′-GGACTCCACTGTCCCTTCAA-3′). *Vangl2^{Lp}* mice and embryos were genotyped as described (Copp et al., 1994). *Sdc4$^{lacZ/+}$;Vangl2$^{Lp/+}$* mice were obtained by natural matings between *Vangl2$^{Lp/+}$* males and *Sdc4$^{lacZ/lacZ}$* females. From the F1 offspring, compound heterozygous mice were selected by genotyping and intercrossed with *Sdc4$^{lacZ/lacZ}$* females to obtain F2 embryos. *Xenopus in vitro* fertilization and microinjection were performed as previously described (Muñoz et al., 2006). The morpholinos used to knockdown Sdc4 were the same as those used previously in our own studies and their specificity has been clearly demonstrated (Muñoz et al., 2006). For knockdown of Vangl2, the morpholino oligonucleotide sequence was 5′-AGTACCGGCT-TTTGTGGCGATCCA-3′. All animal procedures and experiments were performed in accordance with protocols approved by the Pontificia Universidad Católica de Chile Animal Ethics Committee and the Animals (Scientific Procedures) Act 1986 of the UK Government.

Embryo cultures
Embryos from timed matings between *Vangl2$^{Lp/+}$* and wild-type mice (CBA/Ca background) were explanted at E8.5 into Dulbecco's modified Eagle's medium containing 10% fetal calf serum. Culture was in undiluted rat serum, in a roller incubator maintained at 38°C and gassed with a mixture of 5% CO_2/5% O_2/90% N_2, as described previously (Copp et al., 2000). Cultures were stabilized for 1 hour, and then sterile aqueous sodium chlorate was added to a final concentration of 30 mM (1% volume addition) (Yip et al., 2002). The same volume of distilled water was added to control cultures. After 24 hours, embryos were harvested from culture and yolk sacs were processed for genotyping. Embryos were inspected for presence/absence of closure 1, somites were counted and PNP length was measured. Embryos were fixed overnight in ice-cold 4% paraformaldehyde in PBS, before wax embedding and preparation of 7 µm transverse sections, which were stained with Haematoxylin and Eosin.

Immunohistochemistry
Frozen sections (10 µm) were fixed for 10 minutes with 4% paraformaldehyde, blocked for 1 hour at room temperature with 5% inactivated goat serum in PBS + 0.1% Triton (PBST) and immunostained using mouse monoclonal anti-syndecan 4 antibody (Santa Cruz, sc-12766) at a 1:100 dilution or rabbit anti-pan-cadherin antibody (Sigma C3678) at a 1:200 dilution. Slides were then washed in PBST four times for 15 minutes each and primary antibody was detected with appropriate secondary antibodies conjugated to Alexa Fluor 488 or Alexa Fluor 594 (1:1000 dilution; Invitrogen). Sections were mounted in Vectashield and imaged with a FluoView FV1000 confocal microscope.

Whole-mount *in situ* hybridization
Embryos were obtained from time-mated pregnant females and processed for whole mount *in situ* hybridization according to standard protocols. To generate a probe for *Sdc4*, a 543 bp partial cDNA fragment containing a small region of the cytoplasmic domain and the 3′ UTR region was subcloned into pGEM-T easy vector. The *Vangl2* probe was as described previously (Doudney et al., 2005). Antisense and sense cRNA probes were generated by *in vitro* transcription using SP6 RNA polymerase and a DIG RNA Labeling Kit. Whole-mount *Sdc4* embryos were embedded in paraffin wax and sectioned with a microtome at 10 µm. Whole-mount *Vangl2* embryos were embedded in 2% agarose in PBS and sectioned at 50 µm using a vibratome.

Inner-ear dissection, immunostaining and analysis of stereociliary bundle orientation
Temporal bones from E18.5 embryos were fixed for 2 hours in cold 4% paraformaldehyde and cochleae were microdissected. The surrounding cartilage was removed to expose the cochlea, and the anlage of Reissner's membrane was dissected to expose the sensory epithelium. Kinocilia and sensory epithelia were labeled using a monoclonal anti-acetylated tubulin antibody and Texas Red-conjugated phalloidin, respectively. Cochleae were flat mounted in Vectashield and confocal images were obtained with a FluoView FV1000 confocal microscope (Olympus). The orientation of individual stereociliary bundles was determined as described previously (Montcouquiol et al., 2003). Distribution histograms were generated by determining the orientations for individual stereociliary bundles relative to a parallel line to the neural-abneural axis. Measurement of angles was performed using the Screen Protractor 4.0 software. Data were collected from different genotypes obtained from at least three different litters.

Wound healing assays
Analysis of wound repair was performed in 8-week-old mice. To carry out skin excision, the mice were anesthetized, shaved and three equidistant 3 mm diameter skin biopsies were taken with a sterile disposable biopsy punch as described previously (Nishiyama et al., 2011). The wound area was allowed to heal in the open air and photographs were taken every 24 hours. Data were plotted as percentage of open area per day.

Western blot analysis
For overexpression and knockdown experiments, xSdc4-Flag (Muñoz et al., 2006), mVangl2-HA, mVangl2Lp-HA (Gao et al., 2011) and siVangl2 (sc-45595, Santa Cruz Biotechnologies) were used. Cells were grown to 70% confluence in six-well plates and transfected with 2 µg DNA using the calcium phosphate method. After transfection (48 hours), the cells were lyzed with 200 µl lysis buffer A [10 mM Tris (pH 7.5), 150 mM NaCl; 0.5% Triton X-100] containing protease inhibitors and separated by SDS-PAGE, transferred to PVDF membranes, and subjected to immunoblot analysis as described previously (Carvallo et al., 2010). For anti-Stub analysis, experiments were performed as described previously (Carrasco et al., 2005). To determine the half-life of Scd4, Sdc4-Flag cells were transfected and after 2 days were incubated for 0, 1, 3, 5 and 8 hours with 40 µg/ml of cycloheximide. Sdc4 levels were then evaluated by western blot. These experiments were performed in triplicate.

Statistical analysis
Data analyses and statistical analysis for wound healing experiments were performed using Prism 5 software (Graph Pad Software). *P*-values below 0.05 were considered statistically significant. All other statistical analysis was performed using Sigmastat version 3.5.

RESULTS
Syndecan 4 expression during early mouse development
Sdc4 expression during early mouse development was analyzed by whole-mount *in situ* hybridization. At E8-8.5, *Sdc4* is expressed in the cranial neural folds (Fig. 1A) mainly in the cephalic mesenchyme (Fig. 1D). More caudal sections revealed additional expression in the foregut diverticulum and the presumptive cardiac tissue (supplementary material Fig. S1A). At E9.5, the expression in the cephalic mesenchyme is maintained and *Sdc4* transcripts also appear in the neural tube, otic vesicle and hindgut (Fig. 1B,C,E; supplementary material Fig. S1B-D).

For further analysis, we performed staining for β-galactosidase activity in heterozygous embryos (*Sdc4$^{lacZ/+}$*) at E9.0-9.5 and confirmed the expression of *Sdc4* in the neural tube, otic vesicle and hindgut (Fig. 1F,G; supplementary material Fig. S2). Importantly, *lacZ* staining was also prominent in the non-neural ectoderm, mainly on the outside of the open spinal neural folds prior to, and
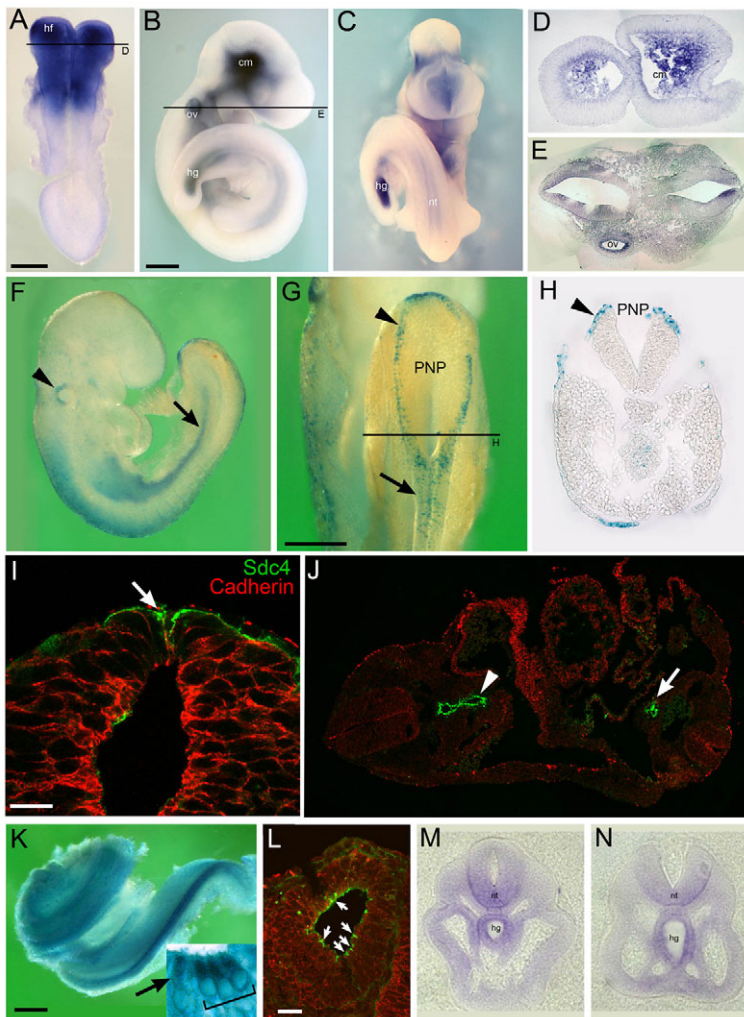
Fig. 1. *Sdc4* and *Vangl2* expression during mouse development. (A-E) Whole-mount *in situ* hybridization with an antisense RNA probe for *Sdc4*. Embryos at E8.5, dorsal view (A), and E9.5, lateral view (B) and rostral view (C). Transverse sections (D,E) are at the levels indicated on embryos in A and B, respectively. (**F-H**) β-Galactosidase activity in *Sdc4^{lacZ/+}* embryos at E9.0. Lateral view (F) shows expression in otic vesicle (arrowhead) and hindgut (arrow). Dorsal view of caudal region (G) shows expression in non-neural ectoderm on the outside of the neural fold of the posterior neuropore (arrowhead) and overlying recently closed neural tube (arrow). Section (H) is from the level indicated by the line in G. Arrowhead indicates the non-neural ectoderm. (**I,J**) Immunostaining of transverse sections through wild-type E9.0 embryos at the hindbrain level using anti-Sdc4 (green, arrows) and anti-pan-cadherin (red). Expression is detected in the neural folds (I, arrow), foregut (J, arrowhead) and hindgut (J, arrow). (**K**) X-Gal staining of the whole cochlea from *Sdc4^{lacZ/+}* embryo at E18.5. Inset: section showing *lacZ* expression in the outer hair cells (bracket) and in the inner hair cell (arrow). (**L**) Immunostaining of Sdc4 (green) on transverse section through the otic vesicle in wild-type E9.0 embryo. (**M,N**) Sections through the closed neural tube (M) and open PNP (N) of an E9.5 embryo subjected to whole-mount *in situ* hybridization using an antisense RNA probe for *Vangl2*. cm, cephalic mesenchyme; hf, head folds; hg, hindgut; nt, neural tube; ov, otic vesicle; PNP, posterior neuropore. Scale bars: 500 μm in A,B; 300 μm in G; 10 μm in I,L; 250 μm in K.

during, closure of the posterior neuropore (Fig. 1G,H). This expression in the non-neural ectoderm was also found by immunofluorescence detection of Sdc4 protein on transverse sections at E9.0 (Fig. 1I), demonstrating expression of Sdc4 in the neural fold during spinal neural tube closure. In addition, Sdc4 protein is also present in the fore and hindgut of E9.5 embryos (Fig. 1J).

At E18.5, Sdc4 expression was detected in the sensory hair cells of the inner ear, particularly in the organ of Corti (Fig. 1K). Detailed analysis suggests that the expression is stronger in the row of three outer hair cells compared with the inner hair cell (Fig. 1K, inset). Immunofluorescence analysis at E9.0 showed expression of Sdc4 protein in the apical pole of the cells in the otic epithelium (Fig. 1L, white arrows).

To compare the expression of *Sdc4* with *Vangl2*, we performed *in situ* hybridization analysis for this component of the PCP pathway. At E9.5, *Vangl2* was expressed in the neural tube (mainly in the ventral side), the hindgut and the otic vesicle (Fig. 1M,N), demonstrating that Sdc4 and Vangl2 are co-expressed, at least in the hindgut and otic vesicle.

In summary, Sdc4 has a dynamic expression pattern during development and is detected in tissues, including the neural tube during and following closure, the hindgut and the cochlea. Co-expression with Vangl2 is consistent with a possible role for Sdc4 in Wnt/PCP signaling during morphogenesis.

Sdc4 and *Vangl2* interact genetically to regulate neural tube closure

Although *Sdc4* knockdown resulted in defective neural tube closure in *Xenopus* embryos (Muñoz et al., 2006), no apparent neural tube defect was detected in *Sdc4*-null mice (Echtermeyer et al., 2001; Ishiguro et al., 2000). To investigate whether total levels of HSPGs might be altered in *Sdc4* knockouts, we used an anti-Stub antibody that recognizes a neo-epitope generated in all HSPG core proteins after treatment with heparitinase. Cell homogenates from mouse embryonic fibroblasts isolated from *Sdc4^{lacZ/lacZ}* mice showed increased levels of a least three other HSPGs (Fig. 2A, see arrows), suggesting that redundancy and compensation could explain the absence of a neural tube closure phenotype in *Sdc4*-null mice.

Thus, we evaluated a possible role for Sdc4 in PCP signaling and neural tube closure by generating *Sdc4;Vangl2* compound mutants. For these studies, we decided to use the *loop-tail* (*Vangl2^{Lp}*) allele as this has a stronger PCP phenotype than other *Vangl2* alleles, including hypomorphic point mutations and a total knockout (Guyot et al., 2011; Yin et al., 2012). Moreover, heterozygotes (*Vangl2^{Lp/+}*) have a weak PCP phenotype that has been extensively used as a sensitized background to detect genes that interact with the PCP pathway (Gao et al., 2011; Lu et al., 2004; Merte et al., 2010; Qian et al., 2007; Yamamoto et al., 2008). Therefore, a genetic interaction with *Vangl2^{Lp/+}* would demonstrate a role for *Sdc4* in Wnt/PCP signaling.
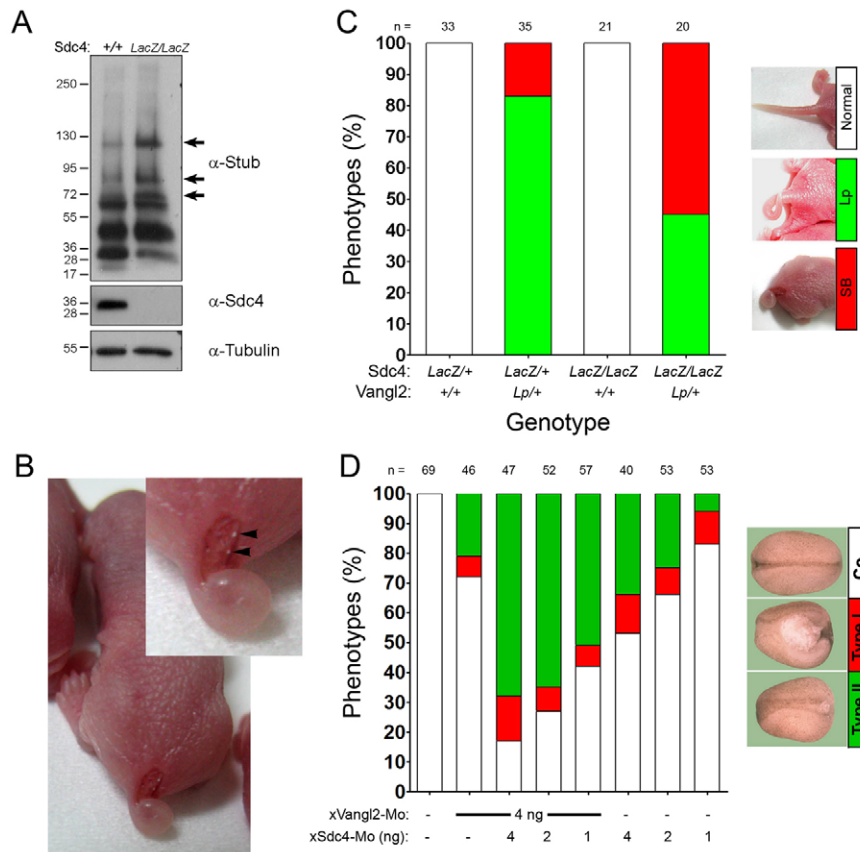
Fig. 2. Genetic interaction between *Sdc4* and *Vangl2* in neural tube closure. (A) HSPGs are upregulated in *Sdc4*-null fibroblasts. Extracts from wild-type or *Sdc4*-null mouse embryonic fibroblasts (MEFs) were analyzed by western blot using anti-Stub, anti-Sdc4 or anti-tubulin antibodies. **(B,C)** Reduction of Sdc4 levels on a *Vangl2$^{Lp/+}$* background results in neural tube defects. (B) A newborn mouse, genotyped as *Sdc4$^{lacZ/lacZ}$;Vangl2$^{Lp/+}$*, exhibiting open sacral spina bifida. The edges of the incomplete neural arches are exposed (arrowheads in magnified view). (C) The incidence of spina bifida in the *Sdc4;Vangl2* compound mice. The number of mice observed with each genotype is given at the top of each bar. The frequency of spina bifida in *Sdc4$^{lacZ/lacZ}$;Vangl2$^{Lp/+}$* mice is significantly greater than in *Sdc4$^{lacZ/+}$;Vangl2$^{Lp/+}$* littermates (Fisher exact test; P=0.006). **(D)** Interaction of *Sdc4* and *xVangl2* in *Xenopus* embryos. Eight-cell stage *Xenopus* embryos were co-injected in the two dorsal-animal blastomeres with the indicated amounts of *Sdc4* and *xVangl2* morpholinos. Phenotypes were classified at stage 20 as type I (severe gastrulation and neural tube closure defects; red) and type II (impairment of neural tube closure; green). The graph summarizes three independent experiments, with numbers of embryos given at the top of each bar. The percentage of embryos with defective neural tube closure is significantly greater with both morpholinos than each morpholino alone (Chi-square test, P<0.001).

To obtain *Sdc4;Vangl2$^{Lp/+}$* compound mutants, we crossed double heterozygous males (*Sdc4$^{lacZ/+}$;Vangl2$^{Lp/+}$*) with *Sdc4$^{lacZ/lacZ}$* females. This protocol was followed to avoid using *Vangl2$^{Lp/+}$* females, almost half of which exhibit imperforate vagina (Murdoch et al., 2001). The number of newborn mice with *Sdc4$^{lacZ/lacZ}$* genotype showed a statistically significant reduction from the expected Mendelian distribution (*P*<0.01) suggesting that loss of Sdc4 function is detrimental to mouse survival (supplementary material Table S1). Importantly, we found that whereas 17% (six out of 35) of *Sdc4$^{lacZ/+}$;Vangl2$^{Lp/+}$* mice were born with a sacral spina bifida (Fig. 2B,C), *Sdc4$^{lacZ/lacZ}$;Vangl2$^{Lp/+}$* mice exhibited a threefold higher frequency of this defect (55%; 11 out of 20), a statistically significant difference (*P*=0.006).

Moreover, in two *Sdc4$^{lacZ/lacZ}$;Vangl2$^{Lp/+}$* mice, a more severe lumbosacral spina bifida was detected (supplementary material Fig. S3). Most of the defective mice also have a looped tail (Fig. 2B,C), as is routinely observed in mice of genotype *Vangl2$^{Lp/+}$* (Copp et al., 1994). In agreement with published results (Echtermeyer et al., 2001; Ishiguro et al., 2000), no defective neural tube closure was observed in mice of *Sdc4$^{lacZ/+}$;Vangl2$^{+/+}$* and *Sdc4$^{lacZ/lacZ}$;Vangl2$^{+/+}$* genotypes (Fig. 2C).

Although the open spina bifida heals at postnatal days 10-15, most of these animals have posterior locomotor defects and are unable to move properly. Importantly, only 12% (2 out of 17) of the *Sdc4$^{lacZ/lacZ}$;Vangl2$^{Lp/+}$* mice survived beyond one postnatal month, compared with 78% survival for *Sdc4$^{lacZ/lacZ}$;Vangl2$^{+/+}$* mice (supplementary material Table S2).

In *Xenopus* embryos, alteration of Wnt/PCP signaling results in CE defects in the mesoderm and neuroectoderm (Wallingford and Harland, 2001). Gain and loss of function of *Sdc4* and *Vangl2* in *Xenopus* embryos disrupts gastrulation and neural tube closure

(Goto and Keller, 2002; Muñoz et al., 2006). To analyze whether Sdc4 and Vangl2 also interact functionally in *Xenopus* embryos, we reduced the endogenous levels of both genes using morpholinos. The effects of these morpholinos could be rescued by overexpression of the respective synthetic mRNA, demonstrating their specificity (Muñoz et al., 2006) (supplementary material Fig. S4). In order to reduce gastrulation defects of the mesoderm (type I phenotype, exogastrulation), the two dorsal animal blastomeres at the eight-cell stage (Wallingford and Harland, 2001) were injected to target the neuroectoderm and produced mainly a defective closure of the neural tube (type II phenotype). Co-injection of suboptimal amounts of Sdc4 and Vangl2 morpholinos (xSdc4-Mo, xVangl2-Mo) resulted in a significantly greater proportion of embryos with defective neural tube closure than the individual morpholinos alone (*P*<0.001; Fig. 2D).

Taken together, these findings demonstrate a genetic interaction between *Sdc4* and *Vangl2*. Based on the role of both genes in Wnt/PCP signaling, we suggest they likely interact in this pathway.

Sdc4 and Vangl2 regulate PCP pathway in cochlear sensory hair cells

Proper polarization and tissue organization of the organ of Corti is one of the clearest examples of PCP in vertebrates (Jones and Chen, 2008). As Sdc4 is expressed in the cochlea, specifically in the hair cells of the organ of Corti (Fig. 1K,L), we analyzed the orientation of the stereocilia in the sensory hair cells. Cochleae were isolated at E18.5, stained with phalloidin (stereocilia) and acetylated tubulin (kinocilium), and analyzed by confocal microscopy. Normal organization of the hair cells was observed in *Sdc4$^{lacZ/+}$;Vangl2$^{+/+}$* mice (Fig. 3A), whereas significant disruption of stereociliary bundle orientation was detected in *Sdc4$^{lacZ/+}$;Vangl2$^{Lp/+}$* and
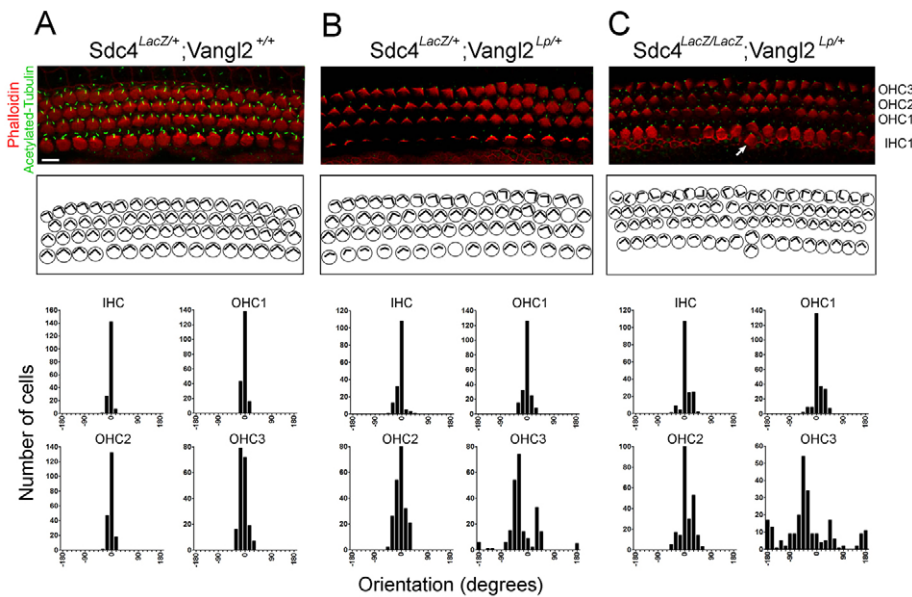
Fig. 3. Sdc4 and Vangl2 interact in cochlear stereociliary bundle orientation. (**A-C**) The interaction between *Sdc4* and *Vangl2* disrupts planar cell polarity in the cochlea. Stereociliary bundles were stained with phalloidin (red) and kinocilia with anti-acetylated-tubulin (green) in cochleae isolated from E18.5 embryos with the indicated genotypes. Arrow indicates supernumerary cells outside the inner hair cell (IHC). Middle panels depict schematic representations of the hair bundle orientation based on the top panel. Bottom panel summarizes the distribution of hair bundle orientation in the IHC, outer hair cell (OHC) 1, OHC2 and OHC3 for each of the three genotypes. Scale bar: 10 µm in A.

$Sdc4^{lacZ/lacZ};Vangl2^{Lp/+}$ mice (Fig. 3B,C). In agreement with the Sdc4 expression pattern (Fig. 1K), the outer hair cell rows 2 and 3 (OHC2, 3) showed more disruption. As with spina bifida, the strongest effect on cochlear morphogenesis was observed in the $Sdc4^{lacZ/lacZ};Vangl2^{Lp/+}$ mice (Fig. 3C), suggesting a dose dependent effect of Sdc4. In addition, supernumerary hair cells, which are also a recognized PCP phenotype (Montcouquiol et al., 2003), were observed in the compound mice and in *Sdc4*-null mice (Fig. 3C and data not shown).

Delayed wound healing in Sdc4 and Vangl2 mutant mice

Sdc4 is upregulated in the epidermis and dermis after wounding (Gallo et al., 1996) and is required for proper wound repair (Bass et al., 2011; Echtermeyer et al., 2001). Moreover, a role for PCP signaling in wound healing has been unveiled by crossing PCP mutants such as *Vangl2* with mice lacking the transcription factor *Grhl3* (Caddy et al., 2010). Based on this, we evaluated a possible interaction between *Sdc4* and *Vangl2* in wound healing.

Excisional wounds were made in the shaved back of 2-month-old mice and the wound area was measured daily for up to 12 days. As reported by Echtermeyer et al. (Echtermeyer et al., 2001), *Sdc4* heterozygous mice showed a small delay in wound closure (Fig. 4C, compare black circles and blue triangles). A much stronger delay in wound healing was detected in *Sdc4;Vangl2* compound mutants (Fig. 4A-C): at 5 days, only 45% of the wound was closed in $Sdc4^{lacZ/+};Vangl2^{Lp/+}$ compared with 75% closure in $Sdc4^{lacZ/+};Vangl2^{+/+}$. Moreover, the wound remained open in the double heterozygous mice at day 9, when it was already closed in the $Sdc4^{lacZ/+};Vangl2^{+/+}$ mice. The fact that even homozygous $Vangl2^{Lp/Lp}$ mice do not have defective wound healing (Caddy et al., 2010), indicates a strong genetic interaction between *Sdc4* and *Vangl2* in wound healing.

Vangl2 regulates Sdc4 steady-state levels

Cellular and biochemical experiments have demonstrated that the $Vangl2^{Lp}$ mutation affects the ability of Vangl2 to interact with Dvls, and adversely affects the subcellular localization and stability of several PCP proteins (Gravel et al., 2010; Iliescu et al., 2011; Merte et al., 2010). Immunofluorescence analysis in HeLa cells with

antibodies against endogenous Sdc4 and Vangl2 showed precise colocalization of both proteins (Fig. 5A). To study the effect of Vangl2 on Sdc4 steady-state levels, HEK293 cells were co-transfected with increasing amounts of Sdc4-Flag DNA and small interfering RNAs designed to inactivate Vangl2 (siVangl2). Western blots were performed after 48 hours. Knockdown of Vangl2 resulted in an increased steady-state level of Sdc4-Flag (Fig. 5B, compare lanes 1, 2 and lanes 4, 5), an effect that was dependent on the amount of Sdc4-Flag expressed (Fig. 5B, compare lane 3 and lane 6). Co-transfection of a mouse version of Vangl2 restored normal
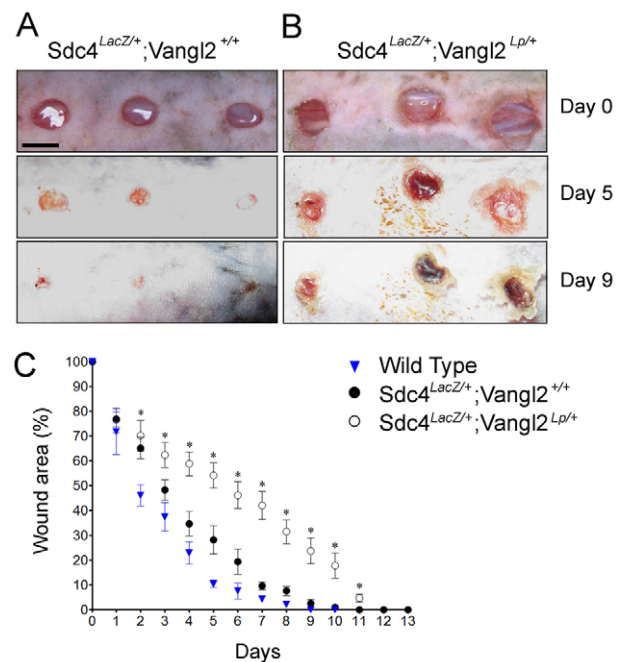

Fig. 4. Sdc4 and Vangl2 interact in wound healing. Wound healing is delayed in *Sdc4;Vangl2* compound mutant mice. (**A,B**) Representative macroscopic views of wound healing in the back skin of mice with the indicated genotypes. (**C**) Summary of the data from a total of at least 9-12 wounds (three or four mice) for each genotype. Data are represented as mean±s.e.m. *$P<0.001$. Scale bar: 3 mm in A.
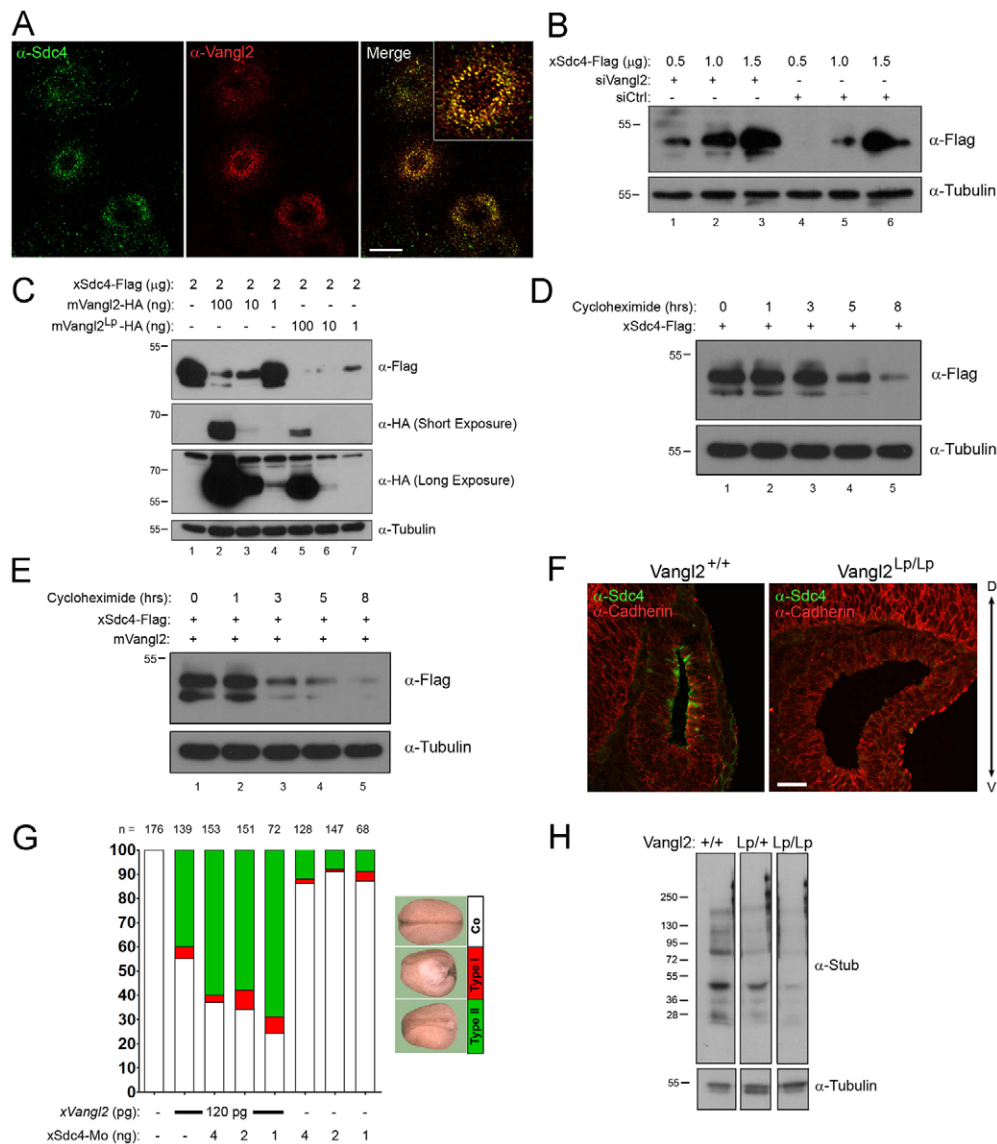
Fig. 5. Vangl2 regulates Sdc4 steady-state levels. (**A**) Sdc4 and Vangl2 colocalize at the subcellular level. Confocal analysis of HeLa cells by double immunofluorescence using antibodies against endogenous Sdc4 (green) and Vangl2 (red). (**B**) siVangl2 increases Sdc4 steady-state levels. HEK293 cells were co-transfected as indicated and xSdc4-Flag steady-state levels were evaluated by western blot. (**C**) Vangl2 reduces Sdc4 steady-state levels. HEK293 cells were co-transfected with the indicated DNAs and xSdc4-Flag steady-state levels were evaluated by western blot. Vangl2^{Lp} is more active than wild-type Vangl2 in this assay. (**D,E**) Cells transfected with xSdc4-Flag (D) without or (E) with mVangl2 were incubated with cycloheximide (40 μg/ml) for different times. The half-life of xSdc4 protein in the different conditions was estimated from experiments in triplicate. (**F**) Sdc4 is absent from otic vesicles of *Vangl2$^{Lp/Lp}$* mice. Double immunofluorescence using antibodies against Sdc4 (green) and pan-cadherin (red) was performed on transverse sections from wild-type and *Vangl2$^{Lp/Lp}$* mutant mice at E9.5. (**G**) Interaction of *Sdc4* and *xVangl2* in *Xenopus* embryos. Eight-cell stage *Xenopus* embryos were co-injected in the two dorsal-animal blastomeres with the indicated amounts of *Sdc4* morpholino and *xVangl2* synthetic mRNA. Phenotypes were classified at stage 20 as type I (severe gastrulation and neural tube closure defects; red) and type II (impairment of neural tube closure; green). The graph summarizes three independent experiments, with numbers of embryos given at the top of each bar. Co-injection of xSdc4-Mo + *xVangl2* mRNA resulted in a significantly greater proportion of embryos with defective neural tube closure than the individual suboptimal amounts of xSdc4-Mo and *xVangl2* mRNA (Chi-square test, *P*<0.001). (**H**) Reduced levels of HSPG in *Vangl2^{Lp}* mice. Homogenates from E14.5 wild-type, *Vangl2$^{Lp/+}$* and *Vangl2$^{Lp/Lp}$* mice were analyzed by western blot using anti-Stub and anti-tubulin antibodies. Scale bars: 10 μm in A; 20 μm in F.

levels of Sdc4, indicating that the effects of siVangl2 were specific (supplementary material Fig. S5A).

In agreement with this, overexpression of Vangl2 decreased Sdc4 steady-state levels, an effect that was dose dependent (Fig. 5C, compare lanes 2-4 and lane 1). A mutant form of Vangl2 that mimics the Lp mutant (mVangl2^{Lp}-HA, Gao et al., 2011) showed the same ability to reduce Sdc4 steady-state levels (Fig. 5C, compare lanes 5-7 and lane 1). Interestingly, Vangl2^{Lp} was even more active than the wild-type Vangl2. Transfection of 1 ng of Vangl2^{Lp} completely abrogated expression of Sdc4, whereas the same amount of Vangl2-HA showed only a partial effect (Fig. 5C, compare lanes 1, 4 and 7). This effect was even more dramatic considering that mVangl2^{Lp}-HA expression levels were lower than the ones of wild-type protein (Fig. 5C, lower panels), a finding that is in agreement with previous reports (Gravel et al., 2010; Iliescu et al., 2011).

The fact that Sdc4 was being overexpressed by transfection of HEK293 cells with an epitope-tagged Sdc4 under the control of a strong CMV promoter suggested that the effect of Vangl2 might be at the post-translational level. To test this prediction, cells overexpressing Sdc4 in the absence or presence of exogenous Vangl2 were incubated for different times with cycloheximide, a protein synthesis inhibitor, and the half-life of Sdc4 was estimated. We found that overexpression of Vangl2 levels reduced the half-life of Sdc4 from 3.2 hours to 2.2 hours (Fig. 5D,E), indicating a direct or indirect effect of Vangl2 at a post-translational level.

To assess the *in vivo* relevance of this observation, we analyzed the effect of Vangl2^{Lp} on Sdc4 levels in wild-type and Vangl2$^{Lp/Lp}$ mice. By immunofluorescence, Sdc4 protein was readily detected in the otic epithelium and non-neural ectoderm of E9.0 Vangl2$^{+/+}$ embryos, whereas no signal could be detected in the otic vesicles and non-neural ectoderm of Vangl2$^{Lp/Lp}$ embryos (Fig. 5F; supplementary material Fig. S6).

In addition to the ability of Vangl2 to regulate Sdc4 steady-state protein level, we also observed the converse: Sdc4 was found to affect Vangl2 steady-state level, as demonstrated using siRNA against Sdc4 (supplementary material Fig. S5B). Taken together, these findings predicted that overexpression of Vangl2 should summate with a knockdown of Sdc4 in *Xenopus* embryos. To test this, we performed an assay similar to the one described in Fig. 2D. The frequency of defective embryos produced by injection of suboptimal amounts of Sdc4 morpholino (1-4 ng) was significantly greater when *xVangl2* was overexpressed by co-injection of synthetic mRNA (Fig. 5G). These results support a mechanism whereby Vangl2 regulates Sdc4 steady-state levels.

Vangl2^{Lp} interacts with overall HSPG expression and function

Our cell transfection and *Xenopus* expression results suggest a mechanism whereby Vangl2 diminishes existing levels of Sdc4 protein, exacerbating Sdc4 reduction and causing a stronger phenotype than partial loss of Sdc4 function alone. However, this explanation is not sufficient to explain the strong interaction observed in Sdc4$^{lacZ/lacZ}$;Vangl2$^{Lp/+}$, where Sdc4 is already completely absent because of the null mutation. Based on the fact that other syndecans, or HSPGs more generally, could compensate for removal of both Sdc4 copies (Fig. 2A), we decided to test a possible effect of Vangl2^{Lp} on overall HSPG expression. Whole E14.5 fetuses were homogenized, and analyzed by western blot using the anti-Stub antibody. As shown in Fig. 5H, all HSPG core proteins were strongly reduced in Vangl2$^{Lp/Lp}$ mutants compared with Vangl2$^{Lp/+}$ and wild type. This suggests that Vangl2^{Lp} has a destabilizing effect on most HSPGs, which provides a mechanistic explanation for the genetic interaction between Sdc4 and Vangl2.

The interaction between Vangl2 and HSPGs could be mediated via the proteoglycan core proteins and/or via the heparan sulfate chains. To test the latter idea, we evaluated the effects of chlorate treatment on Vangl2$^{Lp/+}$ embryos. Chlorate is an inhibitor of proteoglycan sulfation, a modification that is crucial for proteoglycan function. Previously, we have shown that chlorate modulates the rate of spinal neurulation, an effect specifically attributed to diminution of heparan sulfation (Yip et al., 2002). Vangl2$^{Lp/+}$ and wild-type embryos were cultured *in vitro* from E8.5 (fewer than five somites) for 24 hours in the presence or absence of 30 mM sodium chlorate. Strikingly, five out of six Vangl2$^{Lp/+}$ embryos failed to initiate neural tube closure (i.e. closure 1 failure) and developed craniorachischisis (entirely open neural tube). This phenotype is not usually observed in Vangl2$^{Lp/+}$ embryos, whereas
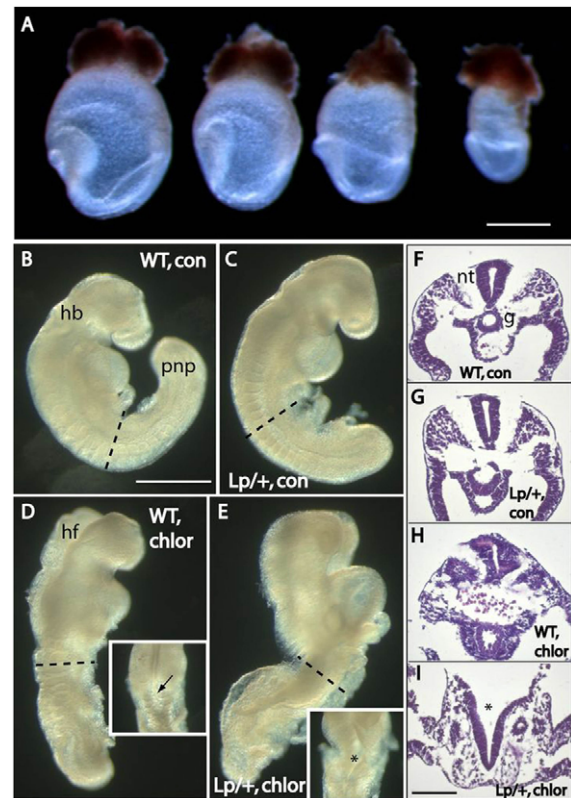

Fig. 6. Inhibition of HSPG sulfation induces severe NTDs in Vangl2$^{Lp/+}$ embryos. Embryos cultured from E8.5 (prior to closure 1) for 24 hours in the presence or absence of sodium chlorate. (**A**) Embryos at E8.5 prior to culture. A range of stages is used: between three somites (left) and no somites (right). (**B,C**) Side views of control (con) embryos after 24 hours culture without chlorate. Both wild-type (B) and Vangl2$^{Lp/+}$ (C) embryos have undergone normal closure 1. Neurulation is nearing completion in the hindbrain, while the posterior neuropore remains open, as expected at this stage. (**D,E**) Side views (with dorsal views in insets) of embryos cultured for 24 hours in chlorate (chlor). Axial rotation is incomplete and cranial neural tube closure is delayed. Despite these abnormalities, the wild-type embryo (D) has undergone closure 1 (arrow in inset), whereas the Vangl2$^{Lp/+}$ embryo (E) has failed in closure 1 (asterisk in inset) and exhibits craniorachischisis. (**F-I**) Transverse sections stained with Haematoxylin and Eosin at the level of the dashed lines in B-E, respectively. A closed neural tube is seen in all groups except the Vangl2$^{Lp/+}$ embryo cultured in chlorate, in which the neural tube is wide open (asterisk in I). The gut has failed to close in this embryo, whereas it is closed in all other embryos. g, gut; hb, hindbrain; hf, open head folds; nt, neural tube; pnp, posterior neuropore. Scale bars: 0.5 mm in A; 0.5 mm in B-E; 0.15 mm in F-I.

it is always present in Vangl2$^{Lp/Lp}$ individuals. Indeed, Vangl2$^{Lp/+}$ embryos cultured in the absence of chlorate exhibited normal closure 1, as did wild-type embryos cultured in chlorate (Fig. 6; Table 1). Hence, there is a gene-environment interaction in which the phenotype of Vangl2$^{Lp/+}$ is converted to that of Vangl2$^{Lp/Lp}$ as a result of suppression of heparan sulfation by chlorate. Based on the fact that Sdc4 expression is not detected at the site of closure initiation (Fig. 1A), and that Vangl2^{Lp} affects the levels of many HSPGs (Fig. 5H), these findings raise the possibility that Vangl2 may interact with other HSPGs in addition to Sdc4.

DISCUSSION

In this study, we report the expression of *Sdc4* during mouse development, its genetic interaction with *Vangl2*, and the finding

Table 1. *Vangl2$^{Lp/+}$* embryos develop severe NTDs when cultured from E8.5 for 24 hours in the presence of sodium chlorate

Treatment	Genotype	Number of embryos	Somite number*	Embryos with CRN (%)[‡]	PNP length[§]
Water	Wild type	6	13.5±1.3	0	0.59±0.05
	Lp/+	5	13.8±1.0	0	0.54±0.02
Na chlorate	Wild type	5	12.2±0.4	0	0.78±0.05
	Lp/+	6	11.2±0.4	83.3	N/A

*Somite number at the end of the culture period (mean±s.e.m.) does not differ significantly between the groups (one-way analysis of variance; $P>0.05$).
[‡]Proportion of embryos with craniorachischisis (CRN) varies significantly between the four groups ($\chi^2=17.3$; $P<0.001$).
[§]Posterior neuropore (PNP) length (mean in mm±s.e.m.) varies significantly among the three groups whose embryos did not exhibit CRN (one-way analysis of variance; $P=0.008$). Wild-type embryos treated with sodium chlorate had significantly longer PNPs than either wild-type or *Lp*/+ embryos exposed to water addition only ($P<0.05$).

that Vangl2 regulates Sdc4 steady-state protein levels. These data suggest that Sdc4 can function within the non-canonical Wnt/PCP signaling pathway. This conclusion is supported by published observations showing that *Sdc4* regulates skeletal muscle regeneration through a PCP/Vangl2-dependent mechanism (Cornelison et al., 2004; Le Grand et al., 2009; Bentzinger et al., 2013).

It is important to consider whether the phenotypes obtained in this study can be attributed solely to the presence of a single copy of the *Vangl2^{Lp}* allele. Although looped tails, occasional spina bifida aperta and a low frequency of defective cochlear hair cell orientation are all found in *Vangl2$^{Lp/+}$* mice (Copp et al., 1994; Yin et al., 2012), we detected a much enhanced frequency and severity of this phenotypic combination in compound *Sdc4;Vangl2* mutants. In particular, *Sdc4$^{lacZ/lacZ}$;Vangl2$^{Lp/+}$* embryos had a much stronger phenotype than *Sdc4$^{lacZ/+}$;Vangl2$^{Lp/+}$* littermates, arguing for a dose-dependent interaction between *Sdc4* and *Vangl2*.

The phenotypes obtained in the *Sdc4$^{lacZ/lacZ}$;Vangl2$^{Lp/+}$* compound mice are consistent with the partially overlapping expression patterns of Sdc4 and Vangl2. Our results and other studies showed that Sdc4 and Vangl2 are both expressed in the cochlea (Torban et al., 2007) and in the epidermis (Gallo et al., 1996; Murdoch et al., 2003; Devenport and Fuchs, 2008), supporting the defective orientation of sensory hairs in the cochlea and delayed wound healing observed in *Sdc4$^{lacZ/lacZ}$;Vangl2$^{Lp/+}$* compound mice. During organogenesis, Sdc4 and Vangl2 are also expressed in the epithelia of many other tissues, including the kidney (N.E., O.C., R.M., M.F., H.C., C.H., U.T., S.E.P., O.W., A.J.C. and J.L., unpublished) (Torban et al., 2007). Interaction at these levels producing defective organ formation could provide an explanation for the diminished survival of *Sdc4;Vangl2* compound mice.

With regard to the neural tube defect phenotypes we observed, the fact that Sdc4 is not expressed at the site of closure initiation (closure 1) at E8.5, whereas Vangl2 is precisely expressed at this site (Ybot-Gonzalez et al., 2007), can explain why *Sdc4$^{lacZ/lacZ}$;Vangl2$^{Lp/+}$* compound mice do not develop craniorachischisis, unlike homozygous Lp mutants. Indeed, when heparan sulfation was inhibited more generally by chlorate, we then observed closure 1 failure in *Vangl2$^{Lp/+}$* embryos.

This leaves unresolved the issue of how Sdc4 and Vangl2 interact to produce the spina bifida phenotype exhibited by the compound mutants. It is interesting to note that the spina bifida in *Sdc4$^{lacZ/lacZ}$;Vangl2$^{Lp/+}$* mice is reminiscent of that observed in the *curly tail* mutant, which carries a hypomorphic mutation of the transcription factor grainyhead-like 3 (*Grhl3*) (Brouns et al., 2011; Gustavsson et al., 2007). In *curly tail*, there is a decrease in cell proliferation specifically in the hindgut (Copp et al., 1988), with a consequent increase in ventral curvature causing mechanical obstruction of PNP closure that results in spina bifida (Brook et al.,

1991). The co-expression of Sdc4 and Vangl2 in the hindgut raises the possibility that imperfect gut morphogenesis could also explain the defective neural tube closure observed in *Sdc4;Vangl2* compound mice. An alternative possibility is that the expression of Sdc4 in the non-neural ectoderm of the spinal neural folds might be important for the development of spina bifida in compound *Sdc4;Vangl2* mutants. A key role for non-neural ectoderm in the process of neural tube closure has been demonstrated in both mice and *Xenopus* (Pyrgaki et al., 2010; Pyrgaki et al., 2011; Morita et al., 2012). However, as Vangl2 expression is not detected in non-neural ectoderm, a non-cell autonomous interaction mechanism would likely be involved in *Sdc4;Vangl2* mutants.

Mechanistically, we have found that Vangl2 can regulate Sdc4 stability. More importantly, the Vangl2^{Lp} mutant protein is extremely potent in reducing Sdc4 levels in embryos as well as in cell culture. Experiments with cycloheximide indicate that the effect of Vangl2 on Sdc4 is at the post-transcriptional level, although whether this is a direct or indirect effect remains an open question. In addition, we found that the levels of other HSPGs are also reduced in *Lp* mutant mice. This coincides with recent findings that the *Lp* mutation disrupts Vangl2 protein trafficking from the endoplasmic reticulum to the plasma membrane (Merte et al., 2010), and that the presence of the Vangl2^{Lp} protein alters the normal localization of other PCP proteins, including Vangl1 and the putative Vangl2-interacting protein Prickle-like2 (Yin et al., 2012). Hence, the *Vangl2^{Lp}* mutation may disturb PCP signaling through an adverse effect on several key interacting proteins, producing a more profound disturbance than loss of Vangl2 alone. Indeed, this putative effect on protein trafficking could also mediate effects of Vangl2^{Lp} through PCP-independent pathways, as suggested by the finding that Vangl2 regulates the cell-surface availability and levels of MMP14 in migrating cells during gastrulation (Williams et al., 2012).

Taken together, our findings provide a potential explanation for the absence of phenotype in the *Sdc4* mutant mice: we suggest that a compensatory mechanism, likely mediated by functional redundancy among HSPGs, may be responsible. Because of its role in non-canonical Wnt signaling, and its interaction with Vangl2 (Marlow et al., 1998), glypican could be a candidate HSPG for this compensatory relationship with Sdc4 loss of function. Although many other HSPGs are upregulated in Sdc4-null fibroblasts, *Lp* mutant mice have reduced HSPG levels. Thus, as Vangl2 is required to regulate the stability of HSPGs, it probably also affects these levels in Sdc4 mice, offering a possible molecular mechanism for the strong phenotype of *Sdc4$^{lacZ/lacZ}$;Vangl2$^{Lp/+}$* mutant mice.

DEVELOPMENT

Author contributions
N.E. participated in the design of the study, carried out most of the experiments, analyzed data and commented on the manuscript. O.C. carried out the cellular and biochemical experiments and participated in wound healing experiments. R.M. performed all the experiments in *Xenopus* embryos. M.F. carried out the embedding and sectioning of embryos, colony maintenance and mouse crosses. H.C. performed the biochemistry experiments. C.H. helped with the genotyping. U.T. helped set up mouse methods and procedures. S.E.P. performed *Vangl2 in situ* hybridization. O.W. participated in the design of the study and revised and commented on the manuscript. A.J.C. performed the embryo culture experiments, participated in the design of the study, data analysis and revised and commented on the manuscript. J.L. participated in the design of the study, supervised the project and wrote the manuscript.

Supplementary material
Supplementary material available online at
http://dev.biologists.org/lookup/suppl/doi:10.1242/dev.091173/-/DC1

References
Bass, M. D., Williamson, R. C., Nunan, R. D., Humphries, J. D., Byron, A., Morgan, M. R., Martin, P. and Humphries, M. J. (2011). A syndecan-4 hair trigger initiates wound healing through caveolin- and RhoG-regulated integrin endocytosis. *Dev. Cell* **21**, 681-693.
Bentzinger, C. F., Wang, Y. X., von Maltzahn, J., Soleimani, V. D., Yin, H. and Rudnicki, M. A. (2013). Fibronectin regulates Wnt7a signaling and satellite cell expansion. *Cell Stem Cell* **12**, 75-87.
Brook, F. A., Shum, A. S., Van Straaten, H. W. and Copp, A. J. (1991). Curvature of the caudal region is responsible for failure of neural tube closure in the curly tail (ct) mouse embryo. *Development* **113**, 671-678.
Brouns, M. R., De Castro, S. C., Terwindt-Rouwenhorst, E. A., Massa, V., Hekking, J. W., Hirst, C. S., Savery, D., Munts, C., Partridge, D., Lamers, W. et al. (2011). Over-expression of Grhl2 causes spina bifida in the Axial defects mutant mouse. *Hum. Mol. Genet.* **20**, 1536-1546.
Caddy, J., Wilanowski, T., Darido, C., Dworkin, S., Ting, S. B., Zhao, Q., Rank, G., Auden, A., Srivastava, S., Papenfuss, T. A. et al. (2010). Epidermal wound repair is regulated by the planar cell polarity signaling pathway. *Dev. Cell* **19**, 138-147.
Carrasco, H., Olivares, G. H., Faunes, F., Oliva, C. and Larraín, J. (2005). Heparan sulfate proteoglycans exert positive and negative effects in Shh activity. *J. Cell. Biochem.* **96**, 831-838.
Carvallo, L., Muñoz, R., Bustos, F., Escobedo, N., Carrasco, H., Olivares, G. and Larraín, J. (2010). Non-canonical Wnt signaling induces ubiquitination and degradation of Syndecan4. *J. Biol. Chem.* **285**, 29546-29555.
Copp, A. J., Brook, F. A. and Roberts, H. J. (1988). A cell-type-specific abnormality of cell proliferation in mutant (curly tail) mouse embryos developing spinal neural tube defects. *Development* **104**, 285-295.
Copp, A. J., Checiu, I. and Henson, J. N. (1994). Developmental basis of severe neural tube defects in the loop-tail (Lp) mutant mouse: use of microsatellite DNA markers to identify embryonic genotype. *Dev. Biol.* **165**, 20-29.
Copp, A., Cogram, P., Fleming, A., Gerrelli, D., Henderson, D., Hynes, A., Kolatsi-Joannou, M., Murdoch, J. and Ybot-Gonzalez, P. (2000). Neurulation and neural tube closure defects. *Methods Mol. Biol.* **136**, 135-160.
Copp, A. J., Greene, N. D. and Murdoch, J. N. (2003). The genetic basis of mammalian neurulation. *Nat. Rev. Genet.* **4**, 784-793.
Cornelison, D. D., Wilcox-Adelman, S. A., Goetinck, P. F., Rauvala, H., Rapraeger, A. C. and Olwin, B. B. (2004). Essential and separable roles for Syndecan-3 and Syndecan-4 in skeletal muscle development and regeneration. *Genes Dev.* **18**, 2231-2236.
Couchman, J. R. (2010). Transmembrane signaling proteoglycans. *Annu. Rev. Cell Dev. Biol.* **26**, 89-114.
Devenport, D. and Fuchs, E. (2008). Planar polarization in embryonic epidermis orchestrates global asymmetric morphogenesis of hair follicles. *Nat. Cell Biol.* **10**, 1257-1268.
Doudney, K., Ybot-Gonzalez, P., Paternotte, C., Stevenson, R. E., Greene, N. D., Moore, G. E., Copp, A. J. and Stanier, P. (2005). Analysis of the planar cell polarity gene Vangl2 and its co-expressed paralogue Vangl1 in neural tube defect patients. *Am. J. Med. Genet. A.* **136**, 90-92.
Echtermeyer, F., Streit, M., Wilcox-Adelman, S., Saoncella, S., Denhez, F., Detmar, M. and Goetinck, P. (2001). Delayed wound repair and impaired angiogenesis in mice lacking syndecan-4. *J. Clin. Invest.* **107**, R9-R14.
Gallo, R., Kim, C., Kokenyesi, R., Adzick, N. S. and Bernfield, M. (1996). Syndecans-1 and -4 are induced during wound repair of neonatal but not fetal skin. *J. Invest. Dermatol.* **107**, 676-683.
Gao, B., Song, H., Bishop, K., Elliot, G., Garrett, L., English, M. A., Andre, P., Robinson, J., Sood, R., Minami, Y. et al. (2011). Wnt signaling gradients establish planar cell polarity by inducing Vangl2 phosphorylation through Ror2. *Dev. Cell* **20**, 163-176.
Goto, T. and Keller, R. (2002). The planar cell polarity gene strabismus regulates convergence and extension and neural fold closure in Xenopus. *Dev. Biol.* **247**, 165-181.
Gravel, M., Iliescu, A., Horth, C., Apuzzo, S. and Gros, P. (2010). Molecular and cellular mechanisms underlying neural tube defects in the loop-tail mutant mouse. *Biochemistry* **49**, 3445-3455.
Gray, R. S., Roszko, I. and Solnica-Krezel, L. (2011). Planar cell polarity: coordinating morphogenetic cell behaviors with embryonic polarity. *Dev. Cell* **21**, 120-133.
Gustavsson, P., Greene, N. D., Lad, D., Pauws, E., de Castro, S. C., Stanier, P. and Copp, A. J. (2007). Increased expression of Grainyhead-like-3 rescues spina bifida in a folate-resistant mouse model. *Hum. Mol. Genet.* **16**, 2640-2646.
Guyot, M. C., Bosoi, C. M., Kharfallah, F., Reynolds, A., Drapeau, P., Justice, M., Gros, P. and Kibar, Z. (2011). A novel hypomorphic Looptail allele at the planar cell polarity Vangl2 gene. *Dev. Dyn.* **240**, 839-849.
Iliescu, A., Gravel, M., Horth, C., Kibar, Z. and Gros, P. (2011). Loss of membrane targeting of Vangl proteins causes neural tube defects. *Biochemistry* **50**, 795-804.
Ishiguro, K., Kadomatsu, K., Kojima, T., Muramatsu, H., Tsuzuki, S., Nakamura, E., Kusugami, K., Saito, H. and Muramatsu, T. (2000). Syndecan-4 deficiency impairs focal adhesion formation only under restricted conditions. *J. Biol. Chem.* **275**, 5249-5252.
Jones, C. and Chen, P. (2008). Primary cilia in planar cell polarity regulation of the inner ear. *Curr. Top. Dev. Biol.* **85**, 197-224.
Kibar, Z., Torban, E., McDearmid, J. R., Reynolds, A., Berghout, J., Mathieu, M., Kirillova, I., De Marco, P., Merello, E., Hayes, J. M. et al. (2007). Mutations in VANGL1 associated with neural-tube defects. *N. Engl. J. Med.* **356**, 1432-1437.
Le Grand, F., Jones, A. E., Seale, V., Scimè, A. and Rudnicki, M. A. (2009). Wnt7a activates the planar cell polarity pathway to drive the symmetric expansion of satellite stem cells. *Cell Stem Cell* **4**, 535-547.
Lu, X., Borchers, A. G., Jolicoeur, C., Rayburn, H., Baker, J. C. and Tessier-Lavigne, M. (2004). PTK7/CCK-4 is a novel regulator of planar cell polarity in vertebrates. *Nature* **430**, 93-98.
Marlow, F., Zwartkruis, F., Malicki, J., Neuhauss, S. C., Abbas, L., Weaver, M., Driever, W. and Solnica-Krezel, L. (1998). Functional interactions of genes mediating convergent extension, knypek and trilobite, during the partitioning of the eye primordium in zebrafish. *Dev. Biol.* **203**, 382-399.
Matthews, H. K., Marchant, L., Carmona-Fontaine, C., Kuriyama, S., Larraín, J., Holt, M. R., Parsons, M. and Mayor, R. (2008). Directional migration of neural crest cells in vivo is regulated by Syndecan-4/Rac1 and non-canonical Wnt signaling/RhoA. *Development* **135**, 1771-1780.
Merte, J., Jensen, D., Wright, K., Sarsfield, S., Wang, Y., Schekman, R. and Ginty, D. D. (2010). Sec24b selectively sorts Vangl2 to regulate planar cell polarity during neural tube closure. *Nat. Cell Biol.* **12**, 41-46.
Montcouquiol, M., Rachel, R. A., Lanford, P. J., Copeland, N. G., Jenkins, N. A. and Kelley, M. W. (2003). Identification of Vangl2 and Scrb1 as planar polarity genes in mammals. *Nature* **423**, 173-177.
Morgan, M. R., Humphries, M. J. and Bass, M. D. (2007). Synergistic control of cell adhesion by integrins and syndecans. *Nat. Rev. Mol. Cell Biol.* **8**, 957-969.
Morita, H., Kajiura-Kobayashi, H., Takagi, C., Yamamoto, T. S., Nonaka, S. and Ueno, N. (2012). Cell movements of the deep layer of non-neural ectoderm underlie complete neural tube closure in Xenopus. *Development* **139**, 1417-1426.
Muñoz, R., Moreno, M., Oliva, C., Orbenes, C. and Larraín, J. (2006). Syndecan-4 regulates non-canonical Wnt signalling and is essential for convergent and extension movements in Xenopus embryos. *Nat. Cell Biol.* **8**, 492-500.
Murdoch, J. N., Doudney, K., Paternotte, C., Copp, A. J. and Stanier, P. (2001). Severe neural tube defects in the loop-tail mouse result from mutation of Lpp1, a novel gene involved in floor plate specification. *Hum. Mol. Genet.* **10**, 2593-2601.

Murdoch, J. N., Henderson, D. J., Doudney, K., Gaston-Massuet, C., Phillips, H. M., Paternotte, C., Arkell, R., Stanier, P. and Copp, A. J. (2003). Disruption of scribble (Scrb1) causes severe neural tube defects in the circletail mouse. *Hum. Mol. Genet.* **12**, 87-98.

Nishiyama, T., Kii, I., Kashima, T. G., Kikuchi, Y., Ohazama, A., Shimazaki, M., Fukayama, M. and Kudo, A. (2011). Delayed re-epithelialization in periostin-deficient mice during cutaneous wound healing. *PLoS ONE* **6**, e18410.

Pyrgaki, C., Trainor, P., Hadjantonakis, A. K. and Niswander, L. (2010). Dynamic imaging of mammalian neural tube closure. *Dev. Biol.* **344**, 941-947.

Pyrgaki, C., Liu, A. and Niswander, L. (2011). Grainyhead-like 2 regulates neural tube closure and adhesion molecule expression during neural fold fusion. *Dev. Biol.* **353**, 38-49.

Qian, D., Jones, C., Rzadzinska, A., Mark, S., Zhang, X., Steel, K. P., Dai, X. and Chen, P. (2007). Wnt5a functions in planar cell polarity regulation in mice. *Dev. Biol.* **306**, 121-133.

Robinson, A., Escuin, S., Doudney, K., Vekemans, M., Stevenson, R. E., Greene, N. D., Copp, A. J. and Stanier, P. (2012). Mutations in the planar cell polarity genes CELSR1 and SCRIB are associated with the severe neural tube defect craniorachischisis. *Hum. Mutat.* **33**, 440-447.

Torban, E., Wang, H. J., Patenaude, A. M., Riccomagno, M., Daniels, E., Epstein, D. and Gros, P. (2007). Tissue, cellular and sub-cellular localization of the Vangl2 protein during embryonic development: effect of the Lp mutation. *Gene Expr. Patterns* **7**, 346-354.

Wallingford, J. B. and Harland, R. M. (2001). Xenopus Dishevelled signaling regulates both neural and mesodermal convergent extension: parallel forces elongating the body axis. *Development* **128**, 2581-2592.

Wallingford, J. B. and Harland, R. M . (2002). Neural tube closure requires Dishevelled-dependent convergent extension of the midline. *Development* **129**, 5815-5825.

Wallingford, J. B., Fraser, S. E. and Harland, R. M. (2002). Convergent extension: the molecular control of polarized cell movement during embryonic development. *Dev. Cell* **2**, 695-706.

Wang, Y. and Nathans, J. (2007). Tissue/planar cell polarity in vertebrates: new insights and new questions. *Development* **134**, 647-658.

Williams, B. B., Cantrell, V. A., Mundell, N. A., Bennett, A. C., Quick, R. E. and Jessen, J. R. (2012). VANGL2 regulates membrane trafficking of MMP14 to control cell polarity and migration. *J. Cell Sci.* **125**, 2141-2147.

Yamamoto, S., Nishimura, O., Misaki, K., Nishita, M., Minami, Y., Yonemura, S., Tarui, H. and Sasaki, H. (2008). Cthrc1 selectively activates the planar cell polarity pathway of Wnt signaling by stabilizing the Wnt-receptor complex. *Dev. Cell* **15**, 23-36.

Ybot-Gonzalez, P., Savery, D., Gerrelli, D., Signore, M., Mitchell, C. E., Faux, C. H., Greene, N. D. and Copp, A. J. (2007). Convergent extension, planar-cell-polarity signalling and initiation of mouse neural tube closure. *Development* **134**, 789-799.

Yin, H., Copley, C. O., Goodrich, L. V. and Deans, M. R. (2012). Comparison of phenotypes between different vangl2 mutants demonstrates dominant effects of the Looptail mutation during hair cell development. *PLoS ONE* **7**, e31988.

Yip, G. W., Ferretti, P. and Copp, A. J. (2002). Heparan sulphate proteoglycans and spinal neurulation in the mouse embryo. *Development* **129**, 2109-2119.